MODELING AND VALIDATION OF MORPHING WING TRAILING EDGE BASED ON ZERO POISSON'S RATIO HONEYCOMB

Shiyong Sun[1,2], Hongzhi Wang[1,2], Rui Yang[1,2] & Qian Wei[3]

[1]School of Mechanical Engineering, Dalian University of Technology, China
[2]State Key Laboratory of High-performance Precision Manufacturing, Dalian University of Technology, China
[3]School of Mechanics and Aerospace Engineering, Dalian University of Technology, China

Abstract

With the development of aviation technology and the further improvement of the requirements on the characteristics of the aircraft such as load carrying, range and maneuvering ability, the flexible deformation of the wing has become an important way to improve the flight performance of the aircraft. Aiming at the design requirements of a variable camber wing, this paper proposes a honeycomb structure with zero Poisson's ratio characteristics and analyzes the influence of the geometric parameters of the honeycomb structure on the equivalent performance. Finally, with the goal of realizing the variable camber wing, the honeycomb structure as the support structure of the wing and the corrugated structure bonded superelastic material as the flexible skin were investigated, and the flexible variable camber wing sample segments were prepared and subjected to deformation tests. The simulation and experimental results were also analyzed and compared in combination with the finite element simulation models. And the feasibility and potential application of the proposed zero Poisson's ratio honeycomb support structure are demonstrated.

Keywords: morphing wing; honeycomb structures; zero Poisson's ratio; equivalent performance

1. General Introduction

Morphing aircraft is a new concept of aircraft based on bird bionics, can be in flight according to the mission, the environment, etc., autonomous adjustment of the wing shape and flight attitude, comprehensively improve its mission adaptability, endurance and maneuverability[1]. The morphing wing is one of the core components of the morphing aircraft to achieve deformation. The key technology for flexible morphing wings is the ability to always keep the skin smooth and continuous, meanwhile to withstand aerodynamic loads[2]. The flexible morphing wing is mainly composed of four main parts: flexible skin, base structure, support structure, and actuator. Among them, the flexible skin and support structure need to ensure that the wing can be flexible and large deformation, fast recovery rate, but also require it to be able to withstand and transfer aerodynamic loads.

In the category of morphing wings, the downward deflection of the trailing edge of the wing not only improves lift, but also reduces the radar reflective area, improves the aerodynamic performance of trans/supersonic aircraft flight, etc. There are many ways to realize a wing with variable trailing edge, such as the finger-type variable camber wing proposed by Pecora et al[3], which can realize independent deflection at the "knuckle". Woods et al[4] proposed a fishbone-type scheme based on bionics, and deformation was achieved by bionic tendon. Currently, the research on the trailing edge of a variable camber wing belongs to the parallel development of mechanical and flexible structures[5].

Honeycomb structure is one of the typical periodic metamaterials characterized by a designable Poisson's ratio, and has become the main load-bearing structure of morphing wings. According to Poisson's ratio properties, honeycomb structures can be categorized into positive Poisson's ratio, negative Poisson's ratio and zero Poisson's ratio structures. Zero Poisson's ratio honeycomb structures can be categorized into having zero Poisson's ratio properties in only one direction and having zero Poisson's ratio properties in both directions based on the Poisson's ratio properties they

exhibit in the face. Zero Poisson's ratio honeycomb structures that are deformable in only one direction are such as the accordion honeycomb structure proposed by Olympio et al[6]. For structures with one-dimensional deformations, the above honeycomb configuration can satisfy the design requirements. However, when deformability is required in both directions, one-dimensional deformed honeycomb structures are no longer applicable, and honeycomb structures that can be deformed in both directions have emerged. For example, Olympio et al. proposed a hybrid positive-negative Poisson's ratio honeycomb structure at the same time as the accordion honeycomb structure[7]. Mohammad Naghavi Zadeh et al[8] proposed a fish cell honeycomb structure that can be applied to morphing skin. Barbarino et al[9] installed cables inside the deformation direction based on a honeycomb structure and realized the wing chord length change by stretching the cables.

In summary, most of the existing zero Poisson's ratio honeycomb structures exhibit zero Poisson's ratio properties in only a single direction. For the increasingly complex deformation needs of morphing structures, a single-direction zero Poisson's ratio honeycomb structure is no longer fully able to meet their needs. Therefore, a honeycomb configuration with zero Poisson's ratio characteristics is proposed in this paper. Based on the analysis of the relationship between the influence of honeycomb geometrical parameters on the equivalent performance, a variable camber wing sample segment is designed and verified by finite element simulation and test. By comparing the simulation and test results, the honeycomb structure has good zero Poisson's ratio characteristics and deformation capability, which broadens the design space of the morphing wing.

2. Novel Zero Poisson's Ratio Honeycomb Structure Design

2.1 Structural Design

Adopting the strategy of deformations canceling each other, the normal re-entrant hexagonal honeycomb (NRHH)[10][11] unit cell is used as the basis for the connecting combinations by folding, so as to obtain the honeycomb structure with zero Poisson's ratio characteristics, as shown in Fig. 1. The core of this honeycomb structure can be viewed as a combination of two parallelograms with the middle overlap removed. When the unit cell is arrayed, it resembles a telescopic shelf along the x-axis and y-axis directions, thus naming the honeycomb configuration of Fig. 1 as a telescopic shelf-type honeycomb structure.

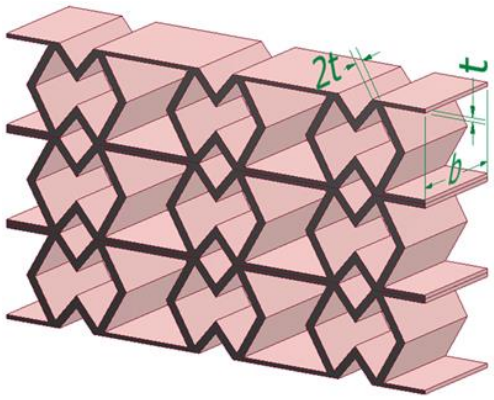

Figure 1 – Novel zero Poisson's ratio honeycomb structure.

2.2 Geometric Parameter

As shown in Figure 2, the geometry of a unit cell of a telescopic shelf-type honeycomb structure can be expressed by the three honeycomb wall lengths H_c, L_1 and L_2, and the angles θ and φ between the two honeycomb sloping walls and the honeycomb horizontal walls. The thickness of the honeycomb wall of the honeycomb structure and the overall thickness of the honeycomb are denoted by t and b. The telescopic shelf-type honeycomb structure can be considered as a concave negative Poisson's ratio honeycomb composed with a positive Poisson's ratio honeycomb structure, so when there is a reasonable combination between the two shapes, the honeycomb structure will have zero Poisson's ratio characteristics. For subsequent ease of analysis, the dimensionless parameters of the telescopic shelf-type honeycomb structure are defined, α, β and λ, the specific parameter definitions are shown in Table 1.

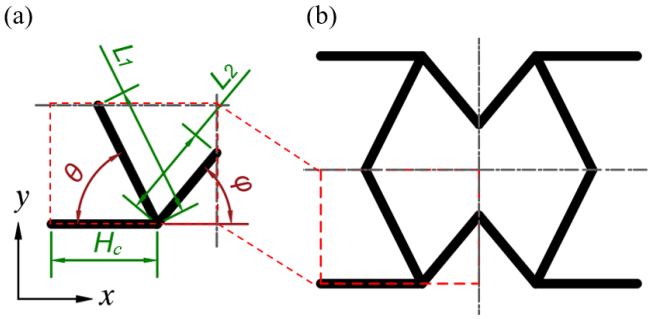

Figure 2 – Geometric schematic and dimensional parameters of honeycomb unit cell.

Table 1 – Definition of dimensionless parameters for telescopic shelf-type honeycomb structures

	Dimensionless parameter	Definition
Telescopic shelf-type honeycomb structures	Ratio of honeycomb sloping wall to straight wall length α	H_c/L_1
	Ratio of honeycomb sloping wall length β	L_2/L_1
	Ratio of honeycomb wall thickness to sloping wall length γ	t/L_1

Since the honeycomb structures are not capable of contacting and penetrating each other, the geometry of the honeycomb should satisfy the following constraints:

$$\begin{cases} 90° > \theta > 0° \\ 90° > \varphi > 0° \\ H_c > L_1 \cos\theta \\ L_1 \sin\theta > L_2 \sin\varphi \end{cases} \xrightarrow{dimensionless} \begin{cases} 90° > \theta > 0° \\ 90° > \varphi > 0° \\ \theta > \arccos\alpha \\ \varphi < \arcsin\left(\sin\theta / \beta\right) \end{cases} \tag{1}$$

Figure 3 shows the feasible domain of this zero Poisson's ratio honeycomb structure. When α and β take different values, the feasible domain of θ and φ is the region enclosed by the upper side of the α straight line and the left side of the β curve and the coordinate axes. It can be deduced under conditions $H_c > L_1 \cos\theta$ and $90° > \theta > 0°$: when $\alpha \geq 1$, the feasible domains of θ and φ are only affected by β, and their feasible domains are the regions bounded by the left-hand side of the β curve and the coordinate axes. And when $1 > \alpha > 0$, the feasible domain of θ and φ is affected by both α and β, it is the region enclosed by the upper side of the α straight line and the left side of the β curve and the coordinate axes. Moreover, as the value of β remains constant and the value of α increases, the feasible domains of θ and φ increase.

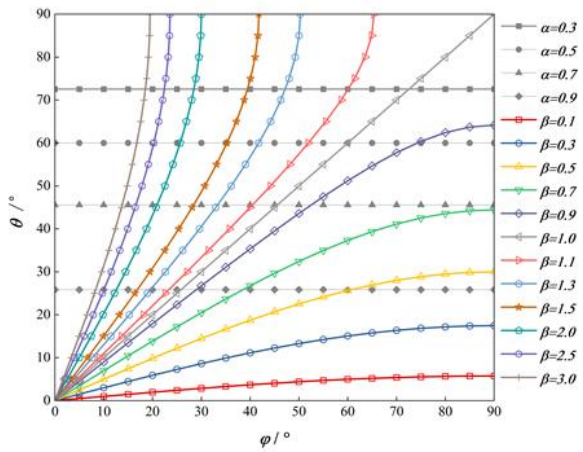

Figure 2 – Feasible domain of zero Poisson's ratio honeycomb structure.

3. Parametric Analysis of Honeycomb Equivalent Properties

3.1 Finite Element Modeling and Analysis Methods

Honeycomb structure is a typical periodic arrangement structure, which is often used as a microstructure in large components. Since the scale of the honeycomb structure is very small relative to the component when it is applied as a microstructure in large components, the analysis using the traditional refined modeling approach often suffers from the problems of difficult modeling and large computational volume. Therefore, this paper analyzes the model of the macroscopic parts by modeling the honeycomb unit cell equivalently and assigning the equivalent parameters to the macroscopic parts as material parameters.

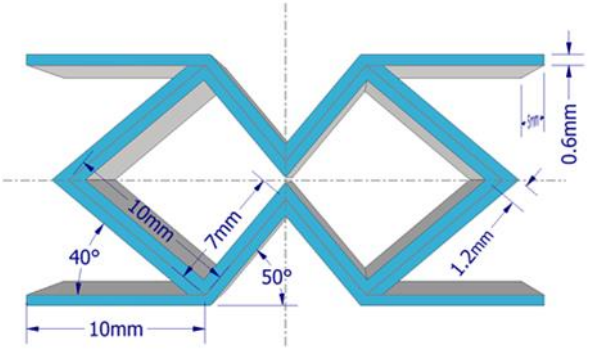

Figure 4 – Dimensions of the fine unit cell mode.

Equivalent modeling analysis was achieved by applying periodic boundary conditions to representative unit cell structures using the Micromechanics Plugin (MMP). A representative unit cell structure refinement model is first constructed based on the proposed novel zero Poisson's ratio honeycomb structure, as shown in Fig. 4. The material was PLA+ with Young's modulus E=1913 MPa and Poisson's ratio of v = 0.35. The characteristic parameters of the honeycomb unit cells are H_c=L_1=10mm, L_2=7mm, $\theta = 40°$, $\varphi = 50°$, t=0.6mm, b=5mm. The elastic modulus, shear modulus, and Poisson's ratio of the representative unit cell structures were calculated by the Micromechanics Plugin, and the results are shown in Table 2.

Table 2 Calculation results of unit cell equivalent performance

E_1(MPa)	E_2(MPa)	E_3(MPa)	v_{12}	v_{13}	v_{23}	G_{12}(MPa)	G_{13}(MPa)	G_{23}(MPa)
38.90	3.83	511.08	0.005	0.027	0.003	0.63	76.44	43.10

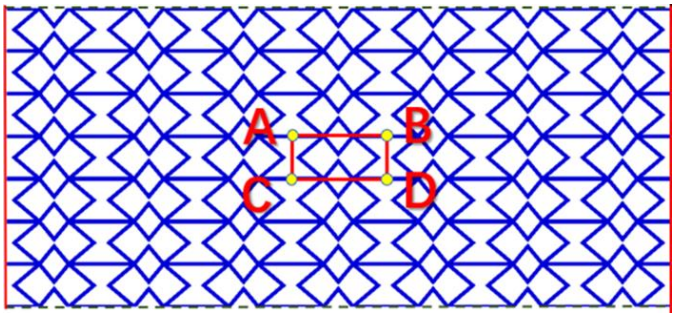

Figure 5 – Refined honeycomb structure model analysis area.

In order to verify the accuracy of the calculation, an equal-size honeycomb structure is built in ABAQUS as a refined model (FEM), and the honeycomb unit cell in the ABCD region of the honeycomb structure is extracted for analysis, as shown in Fig. 5. The material parameters of the finely modeled honeycomb structure are kept constant with the geometric parameters. Axial displacements were applied in the x-direction and y-direction of the honeycomb structure as a whole, respectively, with a displacement value of 0.01 times the length of the unit cell stretching direction. By extracting the displacements at the boundary of the ABCD region and averaging the differences, we can obtain the strain values ε_x and ε_y in the x-direction and y-direction, respectively. The stress values at the boundaries of BD and CD are extracted in the x and y tensile directions, respectively,

and the Poisson's ratio $v_{12} = \varepsilon_2 / \varepsilon_1$ and the modulus of elasticity $E_s = \sigma_s / \varepsilon_s$ are calculated according to the definitions.

The results of the refined simulation model for the equivalent analysis are given in Table 3, as well as the comparison errors with the results calculated by the Micromechanics Plugin. The results can be seen that the error of the elastic modulus of the MMP model relative to the FEM model in both directions is within 10%, and it can be assumed that the results of the MMP model calculations have good accuracy. Compared with refinement modeling, modeling calculations using the Micromechanics Plugin only require equivalent parameter analysis of unit cells of periodic fine-scale structures, which can be used to obtain relatively accurate simulation results by means of material assignment. Therefore, in this paper, all the subsequent discussions on the characteristic parameters of honeycomb unit cells are analyzed using the establishment of the MMP model for equivalent calculations.

Table 3 Refined simulation model equivalent analysis results and errors

Model	E_1	E_2	v_{12}
FEM	36.01	4.07	0.0047
MMP	38.90	3.83	0.0049
Errors	8.01%	-5.93%	3.81%

3.2 Analysis Results of Honeycomb Geometric Parameters

Behnken response surface method was proposed by American statistician R.P. Behnken in 1960 and is mainly used to study the interrelationships between variables in multivariate systems[12]. In order to obtain the influence law of the characteristic geometrical parameters of the honeycomb structure on its equivalent mechanical properties, a unit cell model of the honeycomb structure is established by using the solid unit C3D8R. The finite element simulation plug-in MMP was used to parameterize the honeycomb structure as the original data of the test, and the results were analyzed using the BBD test design method based on the response surface method to obtain the effects of the honeycomb wall angles θ and φ as well as the dimensionless parameters α, β, and γ on the equivalent mechanical properties. The trend surfaces of equivalent elastic modulus, equivalent Poisson's ratio and equivalent shear modulus for their respective high significance parameters are given below.

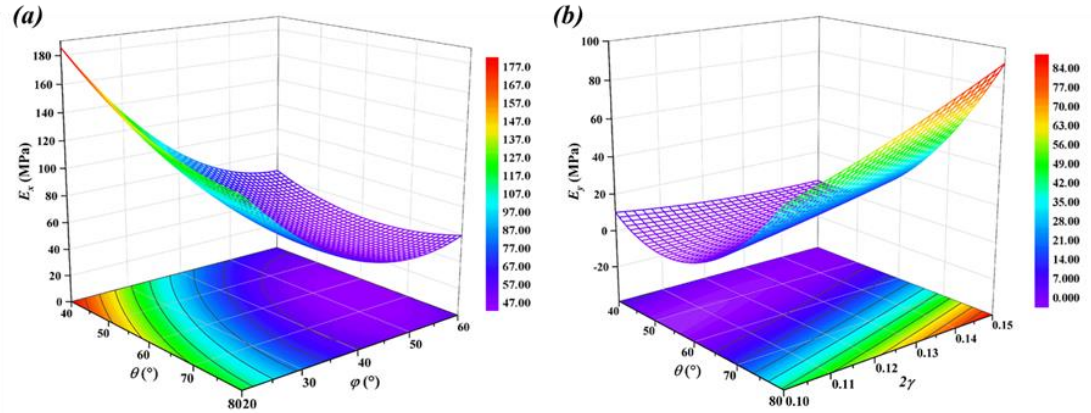

Figure 6 – Effect of honeycomb geometry parameters on equivalent elastic modulus.

From Fig. 6, it can be seen that the trend of honeycomb wall angle φ is more obvious compared to θ, and the smaller the honeycomb wall angle φ is, the larger the elastic modulus E_x is. This is because in the calculation of the elastic modulus E_x, the main stressed honeycomb slant wall is L_2, so the angle φ between this honeycomb slant wall and the straight honeycomb wall has a bigger impact on the elastic modulus E_x. And when φ becomes smaller, the space available for geometrical deformation of the honeycomb structure is smaller, the deformation of honeycomb needs a bigger driving force. The modulus of elasticity E_y is similar to the modulus of elasticity E_x. As θ tends to 90°, there is less space available for geometrical deformation of the honeycomb structure, and the

honeycomb deformation requires a larger driving force, thus the larger the modulus of elasticity E_y.

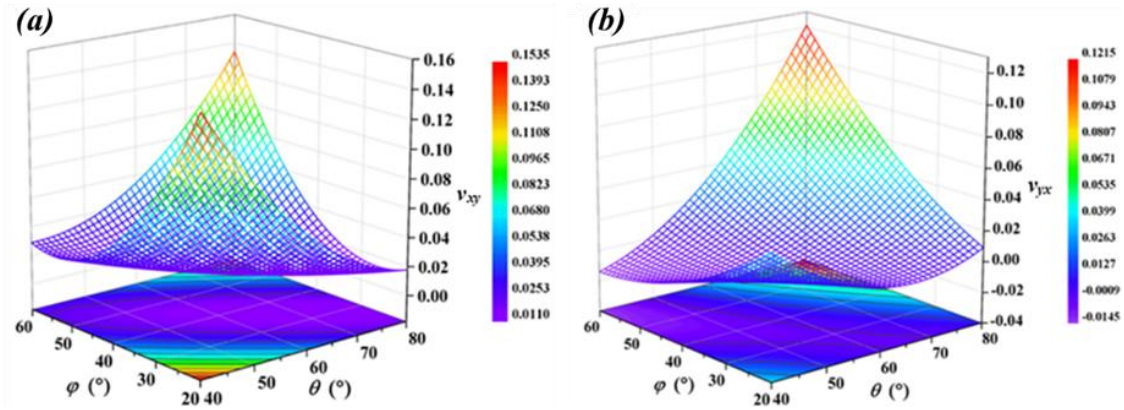

Figure 7 – Effect of honeycomb geometry parameters on equivalent Poisson's ratio.

As can be seen from Fig. 7, the quadratic terms of the honeycomb wall angle θ and φ are both significant, indicating that the relationship between the honeycomb wall angle θ and φ and the Poisson's ratios v_{yx} and v_{xy} is not a linear relationship. The Poisson's ratio is extremely close to 0 when the honeycomb wall angle θ tends to 40° and φ tends to 60° or θ tends to 65° and φ tends to 20°, while when the honeycomb wall angle θ tends to 80° and φ tends to 60°, the Poisson's ratio rises significantly and even the honeycomb structure exhibits a positive Poisson's ratio characteristic. The Poisson's ratio v_{xy} rises more significantly at the limiting position compared to v_{yx}, indicating that the nodal region has a greater influence on the Poisson's ratio in that direction.

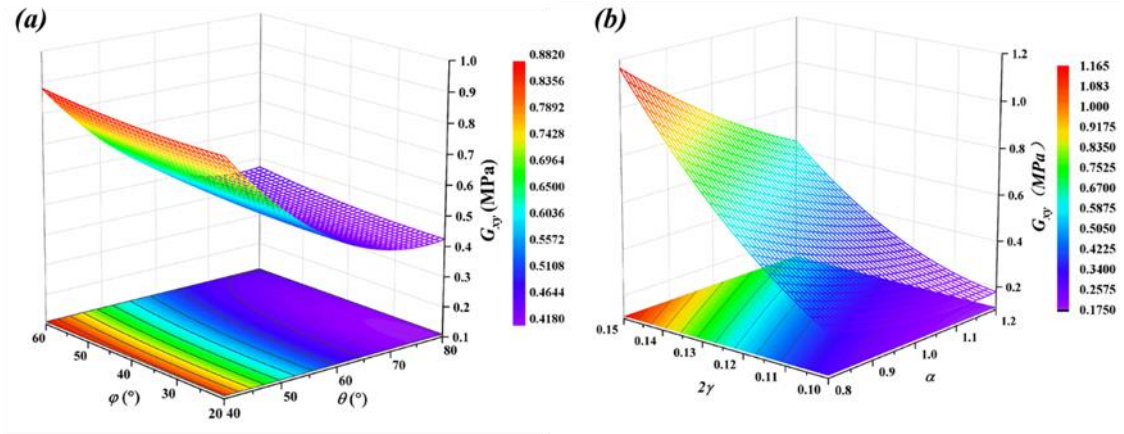

Figure 8 – Effect of honeycomb geometry parameters on equivalent shear modulus.

As shown in Fig. 8, the honeycomb wall angle θ has a more significant effect on the shear modulus G_{xy} compared to φ, and it decreases with the increase of θ angle. For the dimensionless parameter, the shear modulus G_{xy} decreases with the increase of α and the trend increases with the increase of γ.

4. Morphing Camber Wing Based on the Novel Honeycomb.

4.1 Design of morphing camber wing sample segment

In order to verify the actual deformation load bearing characteristics of this honeycomb structure, a morphing camber wing sample segment with an electric actuator as the driving device and the new zero Poisson's ratio honeycomb structure as the supporting structure is designed. Fig. 9 shows the dimensions of the trailing edge morphing camber wing segment, and the profile of the wing segment adopts the NACA0012 symmetric airfoil in the Profili airfoil library, which is mostly used in the design and manufacture of unmanned aerial vehicles (UAV), and is suitable for the study of the morphing camber wing sample segment. The wing has a chord length of 505mm and is divided into three main sections: leading edge, deformation zone, and trailing edge. In particular, the deformation zone is

the main area where the wing sample section achieves morphing, with a length of 34% of the wing chord length.

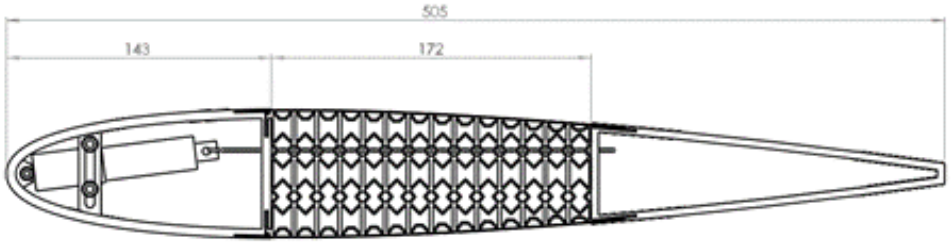

Figure 9 – Dimensions of the constituent areas of the morphing camber wing sample segment.

Figure 10 shows the design of the morphing camber wing. The leading edge part mainly plays the role of fixation, and the leading edge part is completely fixed during the deformation of the wing. The electric actuator is fixed inside the leading edge, and the length of the space inside the leading edge determines the expansion range of the electric actuator. The leading edge is bonded to the deformed area. Considering the poor adhesion of silicone rubber, there is also a snap on the leading edge part to prevent the silicone rubber skin from debonding during stretching. The deformation zone mainly consists of three parts: zero Poisson's ratio honeycomb structure, corrugated structure, and silicone rubber skin. Considering the driving force of the electric actuator and the mechanical properties of the honeycomb structure, the dimensional parameters of the honeycomb structure in the deformation zone are: H_c=L_1=8mm, L_2=4.5mm, $\theta = 45°$, $\varphi = 40°$, t=1mm, b=40mm. The corrugated structure mainly supports the flexible skin, with a wall thickness of 1 mm. The thickness of the silicone rubber skin is 0.5 mm. The trailing edge is connected to the deformation zone by adhesive bonding, and it moves with the rotation of the tail part of the deformation zone. The traction rope leads from the end of the electric actuator, passes through the honeycomb structure of the deformation zone and the trailing edge panel, and is fixed on the panel connecting the trailing edge and the deformation zone.

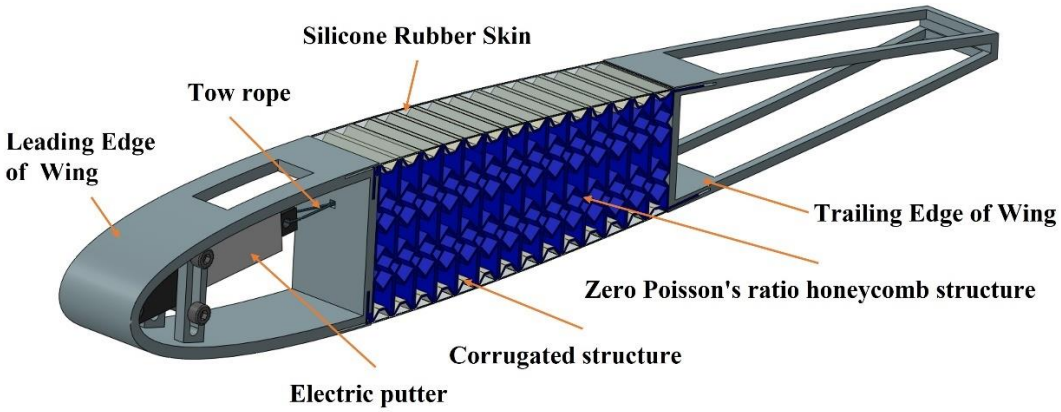

Figure 10 – Morphing camber wing design.

4.2 Finite Element Simulation and Experimental of Morphing Camber Wing Structure

4.2.1 Finite element simulation of morphing camber wing structures

The finite element software ABAQUS is used to simulate the finite element of the morphing camber wing sample segment. Since the leading and trailing edge sections do not participate in the deformation and only change with the change of the middle deformation zone, the leading and trailing edges are set as rigid bodies with a density of 1.18 g/cm^3 in order to reduce the calculation volume. The traction rope material is set to E=206GPa, v=0.24. The deformation zone and upper and lower skin materials are set to be superelastic with hybridization unit C3D8RH. The deformation zone material properties are adopted from the TPU material parameter with a density of 1.21g/cm^3. Silicone rubber material properties and TPU material properties test method is the same, using DIC equipment and material properties tester WDW-1A uniaxial tensile test to obtain the stress-strain

curve for fitting. Considering that the silicone rubber belongs to planar stretching during wing deformation, the planar stretching test was added, as shown in Fig. 11.

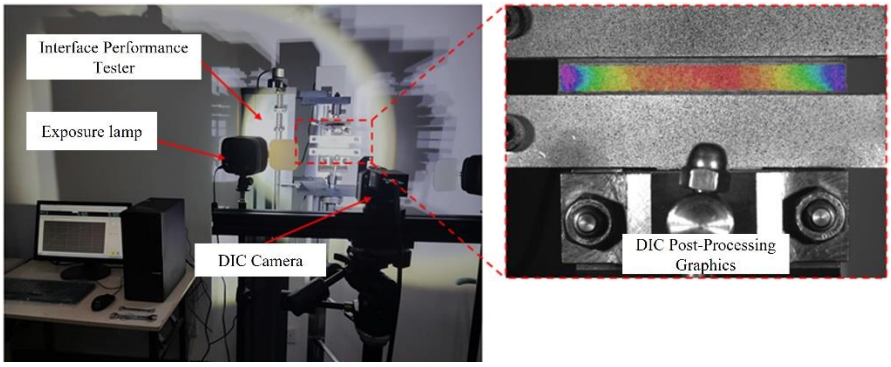

Figure 11 – Schematic diagram of planar tensile experiment of silicone rubber.

Ogden (N=4) was selected as the material constitutive model by fitting the stress-strain curves of uniaxial and planar tensile, and the parameters of the constitutive model are shown in Table 4. The strain energy function for the Ogden model is:

$$W=\sum_{i=1}^{N}\frac{\mu_i}{\alpha_i}\left(\overline{\lambda}_1^{\alpha_i}+\overline{\lambda}_2^{\alpha_i}+\overline{\lambda}_3^{\alpha_i}-3\right)+\sum_{i=1}^{N}\frac{1}{D_k}\left(J-1\right)^{2k} \tag{2}$$

where *N* is the model order, μ_i and α_i are material constants, and *D* is an incompressible parameter used to represent the volume change.

Table 4 Parameters of the constitutive model Ogden (N=4) for silicone rubber materials

N	*μ*	*α*
1	6.46005670	-0.360458435
2	1.974729459e-3	7.36472991
3	-9.97755542	-1.06243840
4	3.84340972	-1.70501812

The simulation is analyzed using implicit dynamics, taking into account the effect of gravity on deformation by fixing the leading edge completely and applying gravity to all other parts of the part. The deformation zone is set to tie constraint with the leading and trailing edges, and the upper and lower skin contact parts. The displacement load to the left is set at the front end of the traction rope, and the tie constraint is set at the end and the trailing edge. Considering that the deformation process, the deformation zone may be penetrated, the self-contact is set between the honeycomb walls which have a large amount of deformation. A reference point is set at the trailing edge end for extracting the displacement value of the wing. The simulation test results of the morphing camber wing sample segment are shown in Fig. 12, and the upward deformation height of the end of the morphing camber wing sample segment is 123.2*mm*.

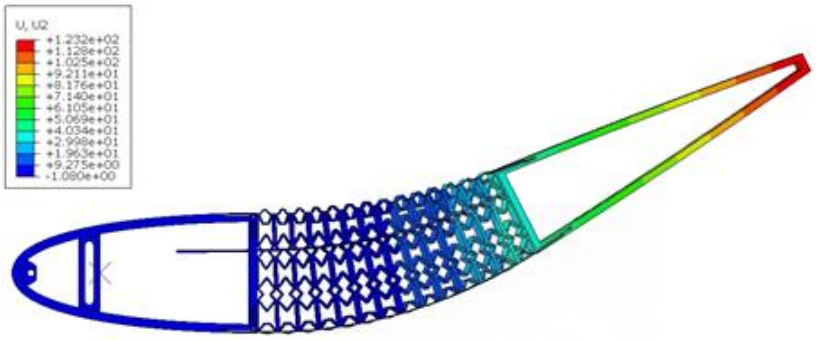

Figure 12 – Finite element cloud diagram of the upward bending height of the morphing camber wing sample segment.

4.2.2 Fabrication and experimental of the sample segment of the morphing camber wing

In order to further verify the actual deformation performance of the honeycomb, the morphing camber wing segment was fabricated and assembled. The leading and trailing edges of the wing section were prepared by Low Force Stereolithography (LFS), and the printing material was a general-purpose resin. The connection area between the honeycomb structure and the corrugated structure is small, in order to prevent the peeling phenomenon of the two during the deformation process, the honeycomb structure and the corrugated structure as a whole are prepared by Fused Deposition Modeling (FDM) technology, and the material is 95A-TPU. Silicone rubber skins are cut to the required size directly from 0.5*mm* thick finished silicone rubber skins. During assembly, the honeycomb-corrugated structure is first bonded to the skin, then the electric actuator is bolted to the inside of the leading edge, and after fixing it, the traction rope is passed through the holes at the end of the electric actuator, and then through the honeycomb structure and the trailing edge part. Finally, the electric actuator is connected to the power supply and governor, so that the electric actuator is in the maximum push-out state, and then the traction rope is tied and fixed at the trailing edge hole. The assembled wing sample segment is shown in Fig. 13.

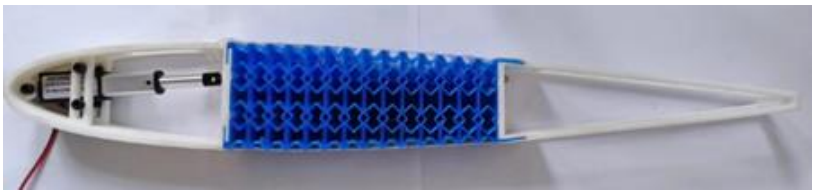

Figure 13 – Morphing camber wing segment test sample.

Fig. 14 shows the upward bending deformation of the wing when the electric actuator is contracted by 30mm. At the initial position, the height gauge is zeroed; when the electric actuator is completely contracted back, the height gauge of the wing upward bending deformation is 119.47*mm*.

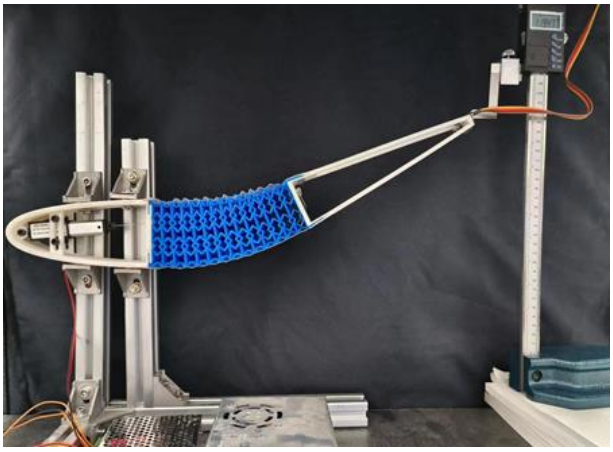

Figure 14 – Upward bending deformation of the wing when the electric actuator is contracted by 30mm.

4.2.3 Finite element simulation and results of equivalent honeycomb wing sample

In order to verify the accuracy of the results of the equivalent elastic parameters, the simulated deformation analysis of the honeycomb structure region after the equivalence of the morphing camber wing is carried out. The deformation zone honeycomb structure is equated to solid blocks of the same size as shown in Fig. 15. Since the morphing camber wing sample segment is mainly subjected to the action of leading and trailing edge clamping surfaces during the deformation process, the material properties of the honeycomb structure after the equivalence are simplified to an isotropic material based on the y-direction of the honeycomb structure. In addition, the effect of strain on the equivalent parameters of the honeycomb structure is particularly pronounced, so the equivalent honeycomb structure is assigned the hyperelastic material performance parameters, the material parameters are shown in Table 5.

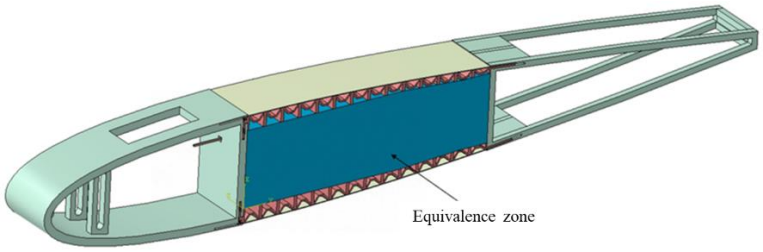

Figure 15 – Sample wing model after honeycomb region equivalence.

Table 5 Equivalent material parameters of honeycomb structure

N	μ	α
1	-0.239700847	2.00005797
2	0.251706745	4.00006545
3	0.037183259	-1.99998799

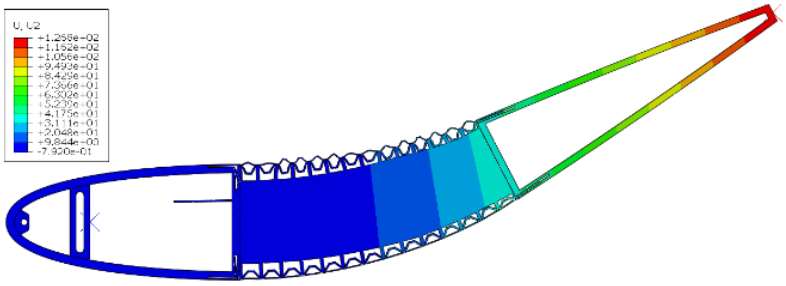

Figure 16 – Schematic diagram of the finite element simulation results of the equivalent model of the morphing camber wing.

Fig. 16 shows the finite element simulation cloud diagram of the morphing camber wing equivalent model. Table 6 shows the experimental results and the refined modeling simulation results, and it can be found that the errors of the results after honeycomb equivalence are 6.14% and 2.92%, respectively. The main reason for the error is that the material properties of the honeycomb equivalent region are simplified, and its material properties are simplified from orthotropic to isotropic materials based on the y-direction of the honeycomb structure, and the material stiffness of the y-direction of the honeycomb structure is much larger than that of the x-direction, which leads to the overall small material properties of the honeycomb structure after the equivalence. Therefore, the simulation results of the end height of the morphing camber wing segment after the equivalence are larger than the actual results.

Table 5 Upward bending height of the end of the morphing camber wing sample segment

Type	Bending height	Error (vs. Experimental)	Error （vs. Refined modeling simulation model）
Experimental	119.47mm	—	—
Refined modeling simulation	123.2mm	3.12%	—
Equivalent simulation	126.8mm	6.14%	2.92%

5. Conclusion

In this paper, a honeycomb structure with zero Poisson's ratio characteristics in the orthogonal directions within the surface is proposed, and the equivalent performance parameters of the honeycomb structure are analyzed by MMP, a finite element simulation plug-in for ABAQUS. With

the goal of realizing the morphing camber wing. A flexible morphing camber wing sample segment with honeycomb structure as the support structure and corrugated structure bonded with superelastic material as the flexible skin was investigated. At the same time of finite element analysis and sample segment preparation, the equivalent model of morphing camber wing sample segment was established to verify the equivalent performance parameters of the honeycomb structure, and the following conclusions were obtained by comparing and analyzing the simulation test results:

1. A honeycomb structure is proposed and has zero Poisson's ratio properties in both orthogonal directions in the face.
2. The relationship between honeycomb wall angles θ and φ and Poisson's ratio v_{yx} and v_{xy} is not a linear relationship, in the case of reasonable choice of honeycomb geometric parameters, can obtain zero Poisson's ratio characteristics honeycomb structure.
3. A morphing camber wing sample segment is designed, and the analysis of the sample segment is carried out by equating the honeycomb structure of the deformation zone to a solid block of the same size, and the errors are 6.14% and 2.92% compared with the experimental results and the refined modeling simulation results, respectively.

6. Contact Author Email Address

Shiyong Sun: sunshy@dlut.edu.cn

Hongzhi Wang: whzhi93@mail.dlut.edu.cn

7. Copyright Statement

References

[1] Hall J, Mohseni K and Lawrence D. Investigation of variable wing-sweep for applications in micro air vehicles. *Proc AIAA Infotech@ Aerospace*, Virginia, 7171, 2005.

[2] Li X J, Liu F, Qiao Y. Development and application prospect of morphing aircraft. *Aircraft Design*, Vol.42, No.5, pp 1-7+13, 2022.

[3] Pecora R. Morphing wing flaps for large civil aircraft: Evolution of a smart technology across the Clean Sky program. *Chinese Journal of Aeronautics*, Vol.34, No.7, pp 13-28, 2021.

[4] Woods B K S, Friswell M I. Preliminary investigation of a fishbone active camber concept. *Proc ASME. SMASIS*, American Society of Mechanical Engineers, Vol.2, 8058, pp 555-563, 2012.

[5] Wang B W, Yang Y, Qian Z S, et al. Technical development of variable camber wing: Review. *Acta Aeronautica et Astronautica Sinica*, Vol.43, No.1, pp024943, 2022.

[6] Olympio K R, Gandhi F. Zero Poisson's ratio cellular honeycombs for flex skins undergoing one-dimensional morphing. *Journal of Intelligent Material Systems and Structures*, Vol.21, No.17, pp 1737-1753, 2010.

[7] Olympio K R, Gandhi F. Zero Poisson's ratio cellular honeycombs for flex skins undergoing one-dimensional morphing. *Journal of Intelligent Material Systems and Structures*, Vol.21, No.17, pp 1737-1753, 2010.

[8] Naghavi Zadeh M, Dayyani I and Yasaee M. Fish Cells, a new zero Poisson's ratio metamaterial—Part I: Design and experiment. *Journal of Intelligent Material Systems and Structures*, 2020, Vol.31, No. 13, pp 1617-1637, 2020.

[9] Barbarino S, Gandhi F and Webster S D. Design of extendable chord sections for morphing helicopter rotor blades. *Journal of Intelligent Material Systems and Structures*, Vol.22, No.9, pp 891-905,2011.

[10] Wang Z. Recent advances in novel metallic honeycomb structure. *Composites Part B: Engineering*, Vol.166, pp 731-741, 2019.

[11] Fu M, Chen Y and Hu L. A novel auxetic honeycomb with enhanced in-plane stiffness and buckling strength. *Composite Structures*, Vol.160, pp 574-585, 2017.

[12] S.L.C Ferreira, R.E. Bruns and H.S. Ferreira. Box-Behnken design: An alternative for the optimization of analytical methods. *Analytica Chimica Acta*, Vol.597, No.2, pp 179-186, 2007.